

Policy Learning for Nonlinear Model Predictive Control with Application to USVs

Rizhong Wang, Huiping Li, *Senior Member, IEEE*, Bin Liang, *Senior Member, IEEE*, Yang Shi, *Fellow, IEEE*, and Demin Xu

Abstract—The unaffordable computation load of nonlinear model predictive control (NMPC) has prevented it for being used in robots with high sampling rates for decades. This paper is concerned with the policy learning problem for nonlinear MPC with system constraints, and its applications to unmanned surface vehicles (USVs), where the nonlinear MPC policy is learned offline and deployed online to resolve the computational complexity issue. A deep neural networks (DNN) based policy learning MPC (PL-MPC) method is proposed to avoid solving nonlinear optimal control problems online. The detailed policy learning method is developed and the PL-MPC algorithm is designed. The strategy to ensure the practical feasibility of policy implementation is proposed, and it is theoretically proved that the closed-loop system under the proposed method is asymptotically stable in probability. In addition, we apply the PL-MPC algorithm successfully to the motion control of USVs. It is shown that the proposed algorithm can be implemented at a sampling rate up to 5Hz with high-precision motion control. The experiment video is available via:https://v.youku.com/v_show/id_XNTkwMTM0NzM5Ng==.html.

Index Terms—policy learning, model predictive control, deep neural networks, constraints, nonlinear systems, unmanned surface vessels (USVs).

I. INTRODUCTION

AS one of the most advanced control technologies, model predictive control (MPC) has been widely used in process control [1], [2]. Recently, MPC strategies have become popular to solve robot control problems because of its optimal control performance and the ability to handle complex system constraints [3]–[5]. However, MPC requires solving an optimal control problem (OCP) periodically online, which is time consuming and cannot guarantee the real-time implementation in robot control applications. This brings great challenges to the application of MPC in the field of robotics [6], [7].

In order to improve the online computational efficiency of OCP, several improved MPC algorithms have been proposed. In [8], the sequential quadratic programming (SQP) optimization strategy is adopted to decrease the computational time of OCP in nonlinear MPC (NMPC). The works in [9] and [10] simplify the nonlinear quadruped robot model to a linear model. In that framework, the original NMPC

optimization problem was replaced by a quadratic program (QP) problem, which can greatly reduce computational burden. In [5], a penalty term is added to the cost function to relax the inequality constraints of OCP, which improves the OCP efficiency.

Another approach to accelerate solution efficiency of OCP is to perform the online MPC optimization process offline. Explicit MPC is a typical method of is this regard [11], [12]. The works in [13] and [14] obtain the explicit solution of the linear MPC optimal problem by solving the multi-parameter QP problem or using the piecewise affine function, respectively. In [15], an approximate explicit MPC control policy is constructed using the barycentric interpolation method, and the system stability and feasibility of the algorithm is theoretically guaranteed. Note that all the above algorithms are only suitable for linear systems. For the non-convex OCP corresponding to the nonlinear system, the explicit MPC is no longer available because of the high computational complexity.

Recently, the learning MPC has become a promising approach to handle OCP based on machine learning [16]. Since the control accuracy of MPC heavily relies on the accuracy of system model, the works in [17]–[19] focused on learning the system model for MPC. Besides, machine learning methods can also assist the design of MPC controller. For example, the works in [20]–[22] used a machine learning method to design the cost function. Alternatively, the work in [23] used the machine learning method to obtain a terminal region of MPC. Besides, machine learning algorithms can also learn the best system constraints of MPC [24], [25]. On the other hand, the MPC can provide expert data for machine learning algorithms. The work in [26] used MPC to guide reinforcement learning (RL) training to improve the training efficiency of RL and guarantee the safety of the RL results.

Different from the traditional machine learning methods, deep neural networks (DNN) have strong capability to learn complex functions and policies. It can be implemented with faster computational speed of forward propagation after appropriate training, without solving complex optimization problems online. Therefore, a promising method to solve the real-time implementation issue of MPC is to use DNNs to learn the control policy offline and then deploy it online. In [27], the primal-dual DNN is used to learn the approximate policy of MPC. To improve the speed of solving large-scale linear MPC, the work in [28] used DNNs to learn the optimal solution, and the system stability and feasibility of optimization problem was guaranteed by primal active sets. The work in [29] utilized the DNN to approximate control policy of robust MPC, and the feasibility and stability of the closed-loop system is also

R. Wang, H. Li and D. Xu are with School of Marine Science and Technology, Northwestern Polytechnical University, Xi'an 710072, China (e-mail: rizhongwang@mail.nwpu.edu.cn; lihuiping@nwpu.edu.cn; xudm@nwpu.edu.cn); B. Liang is with Tsinghua University (bliang@tsinghua.edu.cn); Y. Shi is with Department of Mechanical Engineering, University of Victoria (email:yshi@uvic.ca).

National Natural Science Foundation of China (NSFC) under Grant 61922068, 61733014; Shaanxi Provincial Funds for Distinguished Young Scientists under Grant 2019JC-14; Aoxiang Youth Scholar Program under Grant.

analyzed. In [30], constraint items are added to the traditional DNN to ensure that the approximate policy satisfies the constraints. However, most of the above works are developed for linear systems, which are not suitable for nonlinear systems such as robotic and vehicle systems. In addition, seldom have been implemented and verified via hardware systems.

In this paper, we propose a new policy learning MPC (PL-MPC) scheme for constrained nonlinear systems using DNN and implement it to the motion control of USVs. The main contributions of the paper include:

- We propose a deep supervised learning method to learn the policy of the constrained nonlinear MPC offline to greatly reduce the computational load. The detailed PL-MPC algorithm, the design of the DNN model and its training methods are developed, which provides a feasible tool to deploy nonlinear MPC for robotic control and planning in real-time application.
- We conduct rigorous analysis of the proposed PL-MPC algorithm to make the proposed method theoretically valid. The proximal operator-based optimization and the quadratic penalty method are developed to ensure the practical feasibility of the proposed algorithm. With the PL-MPC algorithm, the closed-loop system is proved to be asymptotically stable in probability under mild conditions.
- We implement the developed PL-MPC algorithm successfully to the motion control of an underactuated USV via lake experiments. The experimental results show that the PL-MPC algorithm can run up to the sampling rate of 5Hz, and the control performance is almost the same as the ideal NMPC in simulation. This verifies the effectiveness and advantage of the proposed policy learning MPC method for robotic.

The rest of this paper is organized as follows: Section II presents the preliminaries and Section III discusses the detailed PL-MPC algorithm. In Section IV, the feasibility of the algorithm and the stability of the closed-loop system are presented. Then real-time experiments on USV motion control with the proposed method are conducted in Section V. Finally, Section VI draws the conclusions.

Notations: In this paper, the following notations are used. The quadratic norm $\mathbf{x}^T \mathbf{Q} \mathbf{x}$ is denoted by $\|\mathbf{x}\|_Q^2$. $[\cdot]$ represents the integer operation, for example, $[x]$ denotes the integer part of x . $[x]^+$ denotes the function $\max(x, 0)$, that is, if $x < 0$, it has $[x]^+ = 0$, otherwise, $[x]^+ = x$. If X is a random variable, $P\{X > x\}$ denotes the probability of $X > x$. $E[X]$ and $V[X]$ represent the expectation and variance of the random variable X , respectively.

II. PRELIMINARIES

A. System Model

Consider a general discrete-time nonlinear dynamic system:

$$\mathbf{x}(k+1) = \mathbf{f}(\mathbf{x}(k), \mathbf{u}(k)). \quad (1)$$

Here, $\mathbf{x}(k) \in \mathbb{R}^n$ and $\mathbf{u}(k) \in \mathbb{R}^m$ are the system state and the control input, respectively. The system state and control input are constrained by the compact sets \mathcal{X} and \mathcal{U} as follows:

$$\begin{aligned} \mathcal{U} &= \{\mathbf{u}(k) \in \mathbb{R}^m \mid \mathbf{u}_{\min} \leq \mathbf{u}(k) \leq \mathbf{u}_{\max}\}, \\ \mathcal{X} &= \{\mathbf{x}(k) \in \mathbb{R}^n \mid \mathbf{g}(\mathbf{x}(k)) \leq \mathbf{0}\}. \end{aligned} \quad (2)$$

We make the following assumptions about sets \mathcal{U} and \mathcal{X} .

Assumption 1: \mathcal{X} is a connected set, and $(\mathbf{0}, \mathbf{0})$ is included within $\mathcal{U} \times \mathcal{X}$.

To facilitate the controller design, the following assumption is made for the system in (1).

Assumption 2: The function $\mathbf{f}(\cdot, \cdot) : \mathbb{R}^n \times \mathbb{R}^m \rightarrow \mathbb{R}^n$ is second-order continuous differentiable, and $\mathbf{0} \in \mathbb{R}^n$ is an equilibrium point of the system, i.e., $\mathbf{f}(\mathbf{0}, \mathbf{0}) = \mathbf{0}$.

B. Optimal Control Problem

For MPC algorithm, the optimization object is a quadratic penalty on the error between predicted system state and control input with the target system state and control input. Without loss of generality, we choose the equilibrium point as the target system state and control input. The cost function is designed as

$$\begin{aligned} J(\mathbf{x}(k), \bar{\mathbf{u}}(\cdot; k)) &= \sum_{i=0}^{N-1} F(\bar{\mathbf{x}}(k+i; k), \bar{\mathbf{u}}(k+i; k)) + V_f(\bar{\mathbf{x}}(k+N; k)) \\ &= \sum_{i=0}^{N-1} (\|\bar{\mathbf{x}}(k+i; k)\|_Q^2 + \|\bar{\mathbf{u}}(k+i; k)\|_R^2) \\ &\quad + \|\bar{\mathbf{x}}(k+N; k)\|_P^2, \end{aligned} \quad (3)$$

where $\bar{\mathbf{u}}(k+i; k)$ and $\bar{\mathbf{x}}(k+i; k)$ are control input sequence and system state sequence under cost function emanating from $\mathbf{x}(k)$. N represents the step of the MPC algorithm in predicting the future state, which is called prediction horizon. $Q \geq 0$, $R \geq 0$ and $P \geq 0$ represent the adjustable weighting matrices of MPC.

Then, OCP is formulated as follows:

Problem P1 :

$$\begin{aligned} \mathbf{u}^*(\cdot; k) &= \arg \min_{\bar{\mathbf{u}}(\cdot; k)} J(\mathbf{x}(k), \bar{\mathbf{u}}(\cdot; k)) \\ \text{s.t. } \bar{\mathbf{x}}(k+i+1; k) &= \mathbf{f}(\bar{\mathbf{x}}(k+i; k), \bar{\mathbf{u}}(k+i; k)) \\ \bar{\mathbf{u}}(k+i; k) &\in \mathcal{U} \\ \bar{\mathbf{x}}(k+i; k) &\in \mathcal{X} \\ \bar{\mathbf{x}}(k+N; k) &\in \mathcal{X}_f, \end{aligned}$$

where $i = 0, \dots, N-1$, $\mathcal{X}_f = \{\mathbf{x} \in \mathbb{R}^n \mid \mathbf{x}^T \mathbf{P} \mathbf{x} \leq \alpha\} \subseteq \mathcal{X}$ is the terminal region, $\mathbf{u}^*(\cdot; k) = \{\mathbf{u}^*(k; k), \mathbf{u}^*(k+1; k), \dots, \mathbf{u}^*(k+N-1; k)\}$ is the optimal control input sequence.

The following standard assumption is made.

Assumption 3: For a system terminal state $\mathbf{x} \in \mathcal{X}_f$, there exists a local stabilizing control policy $\boldsymbol{\kappa}(\mathbf{x}) \in \mathcal{U}$ satisfying

$$V_f(\mathbf{f}(\mathbf{x}, \boldsymbol{\kappa}(\mathbf{x}))) - V_f(\mathbf{x}) \leq -F(\mathbf{x}, \boldsymbol{\kappa}(\mathbf{x})), \quad (4)$$

with $F(\mathbf{x}, \boldsymbol{\kappa}(\mathbf{x})) = \|\mathbf{x}\|_Q^2 + \|\boldsymbol{\kappa}(\mathbf{x})\|_R^2$.

Here, given the initial system state $\mathbf{x}(k)$ and a control sequence $\mathbf{U}(k) = \bar{\mathbf{u}}(\cdot; k)$, the state sequence $\bar{\mathbf{x}}(k+i; k) = \phi(i, \mathbf{U}(k), \mathbf{x}(k))$ satisfies:

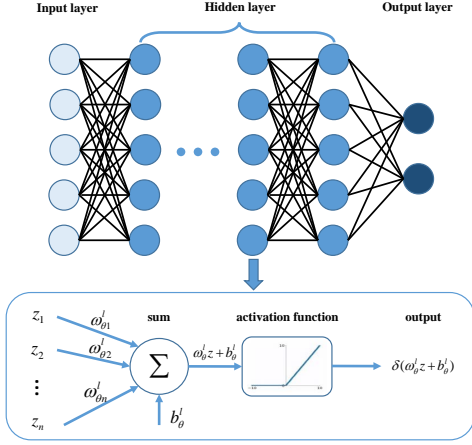


Fig. 1. Feedforward neural networks.

$$\begin{aligned} \phi(i, \mathbf{U}(k), \mathbf{x}(k)) \\ = \mathbf{f}(\dots \mathbf{f}(\mathbf{x}(k), \boldsymbol{\mu}(0, \mathbf{U}(k))), \dots, \boldsymbol{\mu}(i-1, \mathbf{U}(k))), \end{aligned} \quad (5)$$

where $i = 0, \dots, N-1$ and $\boldsymbol{\mu}(i, \mathbf{U}(k)) = \bar{\mathbf{u}}(k+i; k)$.

On this basis, we rewrite problem $\mathcal{P}1$ as the following compact form to facilitate discussions:

Problem $\mathcal{P}2$:

$$\begin{aligned} \mathbf{U}^*(k) &= \arg \min_{\mathbf{U}(k)} J(\mathbf{x}(k), \mathbf{U}(k)) \\ \text{s.t. } \quad &\mathbf{G}(\mathbf{x}(k), \mathbf{U}(k)) \leq \mathbf{0} \\ &\bar{\mathbf{x}}(k+N; k) \in \mathcal{X}_f. \end{aligned}$$

According to (2), $\mathbf{G}(\mathbf{x}(k), \mathbf{U}(k))$ is defined as:

$$\mathbf{G}(\mathbf{x}(k), \mathbf{U}(k)) = \begin{pmatrix} \mathbf{g}(\phi(0, \mathbf{U}(k), \mathbf{x}(k))) \\ \vdots \\ \mathbf{g}(\phi(N-1, \mathbf{U}(k), \mathbf{x}(k))) \\ \boldsymbol{\mu}(0, \mathbf{U}(k)) - \mathbf{u}_{max} \\ \vdots \\ \boldsymbol{\mu}(N-1, \mathbf{U}(k)) - \mathbf{u}_{max} \\ \mathbf{u}_{min} - \boldsymbol{\mu}(0, \mathbf{U}(k)) \\ \vdots \\ \mathbf{u}_{min} - \boldsymbol{\mu}(N-1, \mathbf{U}(k)) \end{pmatrix} \quad (6)$$

C. Feedforward Neural Network

This paper adopts feedforward neural networks (FNN), a type of widely used DNN model, to learn the control policy of NMPC. As shown in figure 1, FNN provides a L-layer neural networks architecture, which forms a mapping from the input \mathbf{z} to the output $\mathbf{f}_\theta(\mathbf{z})$. The detailed formulation is as follows:

$$\mathbf{f}_\theta(\mathbf{z}) = \mathbf{h}_L(\mathbf{h}_{L-1}(\dots \mathbf{h}_2(\mathbf{h}_1(\mathbf{z}))), \quad (7)$$

with the function

$$\mathbf{h}_l(\mathbf{z}) = \delta(\boldsymbol{\omega}_\theta^l \mathbf{z} + \mathbf{b}_\theta^l). \quad (8)$$

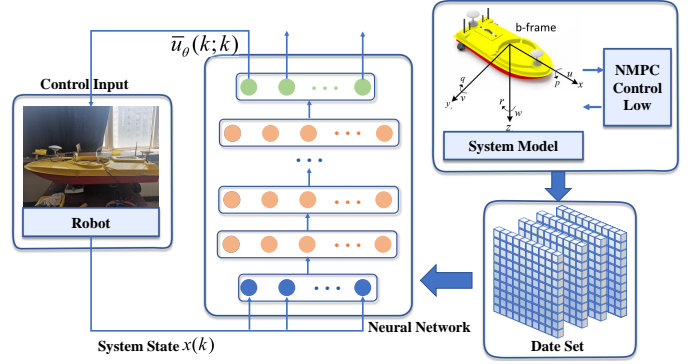


Fig. 2. policy Learning for MPC.

Here, δ is the activation function of DNN. The commonly used activation functions are: sigmoid function $\delta(x) = 1/(1 + e^{-x})$, tanh function $\delta(x) = (2/(1 + e^{-2x})) - 1$ and ReLU function $\delta(x) = \max(0, x)$ [31].

To fitting a function $\mathbf{f}(\mathbf{z}) \in \mathcal{F}$ with the given training data $\{\mathbf{z}^{(i)}, \mathbf{f}(\mathbf{z}^{(i)})\}_{i=1}^M$, the DNN optimizes its parameter $\boldsymbol{\theta} := \{\boldsymbol{\omega}_\theta^l, \mathbf{b}_\theta^l\}_{l=1}^L$ in (8) by minimizing a designed loss function $\mathcal{L}(\cdot)$. It has been proven that the multilayer FNN can approximate any finite discontinuous functions by an arbitrary accuracy [32], [33]. That is, DNN is a universal approximator for Borel measurable function, which is suitable for the NMPC policy learning task in this paper.

III. POLICY LEARNING MPC

A. Policy Learning MPC

In the framework of NMPC, Problem $\mathcal{P}2$ is recursively solved while the new system state $\mathbf{x}(k)$ is obtained, and only the first element of $\mathbf{U}^*(k)$ is applied to the system. Therefore, we can establish a function map between the system state $\mathbf{x}(k)$ and $\mathbf{U}^*(k)$ as follows:

$$\mathbf{U}^*(k) = \boldsymbol{\pi}(\mathbf{x}(k)). \quad (9)$$

Different from the traditional NMPC algorithms utilizing the online optimization method, we use the DNN to fit $\boldsymbol{\pi}(\mathbf{x}(k))$ by $\boldsymbol{\pi}_\theta(\mathbf{x}(k))$ and denote

$$\mathbf{U}_\theta(k) = \boldsymbol{\pi}_\theta(\mathbf{x}(k)), \quad (10)$$

where $\mathbf{U}_\theta(k) = \{\mathbf{u}_\theta(k; k), \mathbf{u}_\theta(k+1; k), \dots, \mathbf{u}_\theta(k+N-1; k)\}$. As introduced in Section II, the parameter $\boldsymbol{\theta}$ of DNN is $\{\boldsymbol{\omega}_\theta^l, \mathbf{b}_\theta^l\}_{l=1}^L$. The detailed policy learning processes for NMPC are shown in Fig. 2.

The loss function of deep learning is designed as

$$\mathcal{L}(\mathbf{U}^*(k), \mathbf{U}_\theta(k)) = J(\mathbf{x}(k), \mathbf{U}_\theta(k)) - J(\mathbf{x}(k), \mathbf{U}^*(k)), \quad (11)$$

so that it can approximate $\boldsymbol{\pi}(\mathbf{x}(k))$ more accurately.

It is straightforward that the loss function $\mathcal{L}(\mathbf{U}^*(k), \mathbf{U}_\theta(k)) \geq 0$ because of the optimality property of $\mathbf{U}^*(k)$. By utilizing the training data set $\mathcal{D} = \{(\mathbf{x}(k), \mathbf{U}^*(k))\}_{k=1}^M$ and the loss function $\mathcal{L}(\mathbf{U}^*(k), \mathbf{U}_\theta(k))$, the supervised learning problem of $\mathbf{U}_\theta(k)$ is converted into the following optimization problem:

$$\theta^* = \arg \min_{\theta} \sum_{k=1}^M \mathcal{L}(\mathbf{U}^*(k), \mathbf{U}_{\theta}(k)). \quad (12)$$

Considering the constraints of system defined in (2), we obtain the following optimization problem:

Problem P3 :

$$\begin{aligned} \theta^* &= \arg \min_{\theta} \sum_{k=1}^M \mathcal{L}(\mathbf{U}^*(k), \mathbf{U}_{\theta}(k)) \\ \text{s.t. } &\mathbf{G}(\mathbf{x}(k), \mathbf{U}_{\theta}(k)) \leq \mathbf{0}. \end{aligned}$$

B. Dual Optimization Learning Algorithm

Traditional learning algorithms only use the unconstrained optimization problems to update θ , which may lead to the failure of the learned control policy in practical implementation because of violating constraints. To deal with this problem, we fulfil the system state and input constraints in P3 by means of Lagrange duality theory [34].

First, an augmented Lagrangian loss function is defined as follows:

$$\begin{aligned} &\mathcal{L}(\mathbf{U}^*(k), \mathbf{U}_{\theta}(k), \mathbf{v}) \\ &= \mathcal{L}(\mathbf{U}^*(k), \mathbf{U}_{\theta}(k)) + \mathbf{v}[\mathbf{G}(\mathbf{x}(k), \mathbf{U}_{\theta}(k))]^+, \end{aligned} \quad (13)$$

where $\mathbf{v} = [v_1, \dots, v_{3N}]$ is the dual variable associated with the constraint $\mathbf{G}(\mathbf{x}(k), \mathbf{U}_{\theta}(k))$.

Then, the dual form of problem P3 is:

Problem P4 :

$$\begin{aligned} \theta^*(\mathbf{v}) &= \arg \min_{\theta} \sum_{k=1}^M \mathcal{L}(\mathbf{U}^*(k), \mathbf{U}_{\theta}(k), \mathbf{v}), \\ \mathbf{v}^* &= \arg \max_{\mathbf{v}} \min_{\theta} \sum_{k=1}^M \mathcal{L}(\mathbf{U}^*(k), \mathbf{U}_{\theta}(k), \mathbf{v}). \end{aligned}$$

Finally, for Problem P4, we integrate the dual gradient descent algorithm and back propagation algorithm to solve it. The concrete steps of the dual optimization learning algorithm is described in Algorithm 1.

Note that \mathbf{v} and θ are designed as an alternative update process in the framework of Algorithm 1. The procedure will be finished once the stopping criteria are satisfied, which means that \mathbf{v} may not converge to the optimal value at the end of iteration. Therefore, although the existence of the dual variable \mathbf{v} encourages parameter θ to converge to the approximate optimal value while satisfying the constraints in the process of updating, the non-optimal value \mathbf{v} would lead to a slight violation of the constraints in probability. This issue will be further discussed and tackled in Section IV-A.

C. PL-MPC Algorithm

The approximate control policy $\pi_{\theta}(\mathbf{x}(k))$ is learned through the training dataset. In order to have a more comprehensive learning control policy, we need training samples that can cover the whole feasible region of MPC.

We use a rejection random sampling algorithm to sample the initial state $\mathbf{x}(0)$ of control trajectories in the feasible region. In order to reduce the similarity of the samplings and improve

Algorithm 1 Dual Optimization Learning Algorithm

Require: Initial training dataset $\mathcal{D} = \{(\mathbf{x}(k), \mathbf{U}^*(k))\}_{k=1}^M$, initial DNN parameter θ , initial optimal step size of DNN ε , initial dual variable \mathbf{v} , initial dual updated step size $\alpha = \{\alpha_0, \alpha_1, \dots\}$.

for each $j = 0, 1, 2, \dots$ **do**

while Loss function gradient greater than expected **do**

Randomly sample m small batch samples $\{(\mathbf{x}(1), \mathbf{U}^*(1)), \dots, (\mathbf{x}(m), \mathbf{U}^*(m))\} \in \mathcal{D}$

Calculate the output of the DNN in system state $\mathbf{x}(k)$: $\mathbf{U}_{\theta}(k) = \pi_{\theta}(\mathbf{x}_k)$

Calculate $J(\mathbf{x}(k), \mathbf{U}_{\theta}(k))$ and $J(\mathbf{x}(k), \mathbf{U}^*(k))$ using (1) and (3).

Calculate $\mathcal{L}(\mathbf{U}^*(k), \mathbf{U}_{\theta}(k))$ using (11).

Convert the dual form $\mathcal{L}(\mathbf{U}^*(k), \mathbf{U}_{\theta}(k), \mathbf{v}^j)$ using to (13).

Calculate the average loss functions of m Samples $\frac{1}{m} \sum_{k=0}^m \mathcal{L}(\mathbf{U}^*(k), \mathbf{U}_{\theta}(k), \mathbf{v}^j)$.

Calculate the gradient of the average loss functions $\nabla_{\theta} \frac{1}{m} \sum_{k=0}^m \mathcal{L}(\mathbf{U}^*(k), \mathbf{U}_{\theta}(k), \mathbf{v}^j)$ for parameter θ .

Update parameters $\theta \leftarrow \theta - \varepsilon \nabla_{\theta} \frac{1}{m} \sum_{k=0}^m \mathcal{L}(\mathbf{U}^*(k), \mathbf{U}_{\theta}(k), \mathbf{v}^j)$

end while

Update the Lagrangian dual variable $v_i^{j+1} \leftarrow v_i^j + \alpha_j \sum_{k=1}^n [\mathbf{G}_i(\mathbf{x}(k), \mathbf{U}_{\theta}(k))]^+ \quad i \in \{1, 2, \dots, 3N\}$

end for

the coverage of samples in the feasible region, we determine whether to adopt the new sample by comparing the distance between the new sample $\mathbf{x}^k(0)$ and the existing one.

Assuming that there are h existing samples $\{\mathbf{x}^1(0), \mathbf{x}^2(0), \dots, \mathbf{x}^h(0)\}$, their center of gravity can be expressed as:

$$\mathbf{x}^g(0) = \frac{1}{h} \sum_{i=1}^h \mathbf{x}^i(0). \quad (14)$$

We can get the distance from the new sampling point \mathbf{x}_0^k to the center of gravity \mathbf{x}_0^g as:

$$dis = \|\mathbf{x}^k(0) - \mathbf{x}^g(0)\|_2. \quad (15)$$

If $dis > \tau_k$ is satisfied, $\mathbf{x}^k(0)$ is taken as the new initial point, otherwise the initial point will be sampled again. The minimum distance τ_k decreases with the increase of sampling number k as

$$\tau_k = \gamma^{\lfloor \frac{k}{K} \rfloor} \tau. \quad (16)$$

Here, $\tau > 0$ is a constant value used to filter the near sampling points and γ is a discount factor satisfying $0 < \gamma < 1$. K is a positive integer, which means that τ_k is updated every K samples.

Next, the center of gravity is updated as follows:

$$\mathbf{x}^g(0) = \frac{1}{k} \mathbf{x}^k(0) + \frac{k-1}{k} \mathbf{x}^g(0). \quad (17)$$

Using the above algorithm, we obtain a series of initial points $\mathbf{x}(0)$. In order to obtain training samples, we use the

NMPC algorithm to get L-step control trajectory $\tau(\mathbf{x}(0)) = \{(\mathbf{x}(0), \mathbf{U}^*(0)), (\mathbf{x}(1), \mathbf{U}^*(1)), \dots, (\mathbf{x}(L), \mathbf{U}^*(L))\}$. We combine control trajectory from H different initial states to get the training dataset

$$\mathcal{D} = \tau(\mathbf{x}^1(0)) \cup \tau(\mathbf{x}^2(0)) \cup \dots \cup \tau(\mathbf{x}^H(0)). \quad (18)$$

The same method is used to generate the test set for supervised learning.

There is a correlation between the sample data obtained by the above method, because the control trajectory is obtained in time sequence. In order to break the association of training data and make it independent and identically distributed (i.i.d), we use a data buffer to store and uniform randomly sample training data.

The training goal of the supervised learning algorithm is that the empirical error of the DNN loss function reaches the expected value. We reduce the empirical error of DNN training by increasing the number of training samples in the training dataset and increasing the number of training steps, until the experience error satisfies the condition.

When the DNN is trained, it will be deployed into the controller. To ensure stability, design the state region $\mathcal{X}_0 = \{\mathbf{x} \in \mathbb{R}^n | \mathbf{x}^T \mathbf{Q} \mathbf{x} \leq \gamma \alpha\} \subseteq \mathcal{X}_f$, where $\gamma \in (0, 1)$. If $\mathbf{x}(k) \in \mathcal{X}_0$, there exists $\mathbf{u}(k) = \kappa(\mathbf{x}(k))$, otherwise use approximate control policy $\pi_\theta(\mathbf{x}(k))$. The detailed learning algorithm is presented in Algorithm 2.

Algorithm 2 PL-MPC Algorithm

Require: Initialize training data buffer.

Offline:

Use rejection random sampling sampling method to randomly sample initial state $\mathbf{x}(0)$.

Control trajectory $\tau(\mathbf{x}(0))$ obtained by NMPC algorithm.

Store Control trajectory data in data buffer.

Collect batch data from data buffer.

Train DNN Using Algorithm 1.

Verify the learning effect by using empirical error

if The empirical error is less than the expected error **then**

Stop training.

return The approximate control policy π_θ .

else

Return to offline step 1 and continue training.

end if

Online:

for $k = 0, 1, 2, 3, \dots$ **do**

Obtain the state of the controlled object $\mathbf{x}(k)$.

if $\mathbf{x}(k) \in \mathcal{X}_0$ **then**

Set control input $\mathbf{u}(k) = \kappa(\mathbf{x}(k))$.

else

Set N control sequences $\mathbf{U}(k) = \bar{\mathbf{u}}(\cdot; k) = \pi_\theta(\mathbf{x}(k))$.

Set control input $\mathbf{u}(k) = \bar{\mathbf{u}}(k; k)$.

end if

end for

IV. FEASIBILITY HANDLING AND STABILITY ANALYSIS

A. Feasibility Handling

This subsection deals with the constraint satisfaction issue of Problem $\mathcal{P}3$ to ensure the feasibility of the proposed Algorithm 2. As mentioned at the end of Section III-B, although the dual optimization learning algorithm provides an effective method to handle the constraints of PL-MPC, there exists a small chance that the approximate solution may violate constraints. In this particular case, we use the proximal operator to guarantee the feasibility of PL-MPC algorithm.

By adding a projection mapping layer on the basis of the original DNN, the proximal operator is able to translate the approximate solution $\mathbf{U}_p(k)$ generated by DNN into a high-quality feasible solution $\mathbf{U}_\theta(k)$. The projection mapping layer is designed as follows:

Problem $\mathcal{P}5$:

$$\begin{aligned} & \arg \min_{\mathbf{U}_\theta(k)} \|\mathbf{U}_\theta(k) - \mathbf{U}_p(k)\|_2 \\ & \text{s.t. } \mathbf{G}(\mathbf{x}(k), \mathbf{U}_\theta(k)) \leq \mathbf{0}. \end{aligned} \quad (19)$$

Generally, $\mathbf{U}_p(k)$ belongs to the feasible region by using the dual optimization learning algorithm, i.e., $\mathbf{U}_\theta(k) = \mathbf{U}_p(k)$. When the approximate solution $\mathbf{U}_p(k)$ does not exist in the feasible region, we can obtain the corresponding feasible solution $\mathbf{U}_\theta(k)$ by solving the optimization problem $\mathcal{P}5$.

Here, the problem $\mathcal{P}5$ is solved through exterior point penalty function methods. Define a penalty function as:

$$\mathbf{Q}(\mathbf{U}_\theta(k), \mu) = \|\mathbf{U}_\theta(k) - \mathbf{U}_p(k)\|_2 + \mu([\mathbf{G}(\mathbf{x}(k), \mathbf{U}_\theta(k))]^+)^2, \quad (20)$$

where $\mu > \mathbf{0}$ is the penalty parameter. Obviously, as the increase of μ , the penalty function $\mathbf{Q}(\mathbf{U}_\theta(k), \mu)$ will be far away from the optimal value $\mathbf{Q}(\mathbf{U}_\theta^*(k), \mu)$ if $\mathbf{U}_\theta(k)$ violates the constraint $\mathbf{G}(\mathbf{x}(k), \mathbf{U}_\theta(k)) \leq \mathbf{0}$, which makes the unconstrained problem $\arg \min_{\mathbf{U}_\theta(k)} \mathbf{Q}(\mathbf{U}_\theta(k), \mu)$ equivalent to problem $\mathcal{P}5$. The detailed quadratic penalty method is presented in Algorithm 3.

Algorithm 3 Quadratic Penalty Method

Require: Initialize $\mu_0 = 1$ and γ , starting point $\mathbf{U}_\theta^0(k) = \mathbf{U}_p(k)$ and $\xi > 0$.

for $i = 0, 1, 2, 3, \dots$ **do**

Optimize $\mathbf{Q}(\mathbf{U}_\theta(k), \mu_i)$ under $\mathbf{U}_\theta(k)$ starting at $\mathbf{U}_\theta^i(k)$, until $\|\nabla_{\mathbf{u}} \mathbf{Q}(\mathbf{U}_\theta(k), \mu_i)\| < \xi$.

if satisfy restraint condition **then**

break.

end if

$\mu_{i+1} = \gamma \mu_i$.

Choose new starting point $\mathbf{U}_\theta^i(k)$.

end for

Now, by integrating the dual optimization learning algorithm and the proximal operator, there always exists a feasible solution for the problem $\mathcal{P}3$.

Remark 1: Note that after the pre-processing of $\mathbf{U}_p(k)$ by the dual optimization learning algorithm, $\mathbf{U}_p(k)$ is not

far away from $\mathbf{U}_\theta(k)$ in the case of constraint violations. Therefore, a small number of iterations are required to find $\mathbf{U}_\theta(k)$ in Algorithm 3, which can still obtain a fast solution without much computation resources.

B. Stability Analysis

In this subsection, we develop the stability result of the closed-loop system for the proposed learning algorithm.

We start with considering the loss function in (11) with the learned control policy \mathbf{U}_θ designed in this paper. To improve the control performance of the proposed algorithm, we require the loss function to be less than a positive real number $\varepsilon > 0$,

$$\mathcal{L}(\mathbf{U}_\theta, \mathbf{U}^*) < \varepsilon. \quad (21)$$

In the policy learning procedure, due to the randomness of learning data and samples, the loss function $\mathcal{L}(\mathbf{U}_\theta, \mathbf{U}^*)$ is a random variable. In what follows, we develop a result ensuring (21) holds in probability.

Theorem 1: Suppose the training data input $\mathbf{x}(k)$ satisfies the uniform distribution and the training data samples are sampled independently from this distribution. For the learned control policy \mathbf{U}_θ generated by Algorithm 2 and the optimal one \mathbf{U}^* , given $\delta \in (0, 1]$ and $\varepsilon > 0$, there exists a large number of training samples M , such that:

$$P\{\mathcal{L}(\mathbf{U}_\theta, \mathbf{U}^*) < \varepsilon\} \geq 1 - \frac{R_{emp}(\mathbf{U}_\theta, \mathbf{U}^*)}{(1 - \sqrt{\frac{c-1}{M\delta}})\varepsilon}, \quad (22)$$

where $R_{emp}(\mathbf{U}_\theta, \mathbf{U}^*)$ is the empirical error of M training data samples defined as follows:

$$\begin{aligned} R_{emp}(\mathbf{U}_\theta, \mathbf{U}^*) \\ = \frac{1}{M} \sum_{k=1}^M (J(\mathbf{x}(k), \mathbf{U}_\theta(k)) - J(\mathbf{x}(k), \mathbf{U}^*(k))), \end{aligned} \quad (23)$$

c is a constant value satisfying $c \geq 1$.

Proof 1: Considering the nonnegativity of $\mathcal{L}(\mathbf{U}_\theta, \mathbf{U}^*)$ and applying the Markov's Inequality to it for $\varepsilon > 0$, we have:

$$P\{\mathcal{L}(\mathbf{U}_\theta, \mathbf{U}^*) \geq \varepsilon\} \leq \frac{E[\mathcal{L}(\mathbf{U}_\theta, \mathbf{U}^*)]}{\varepsilon}, \quad (24)$$

where $E[\mathcal{L}(\mathbf{U}_\theta, \mathbf{U}^*)]$ is the generalization error of the learning algorithm defined as [36]:

$$\begin{aligned} E[\mathcal{L}(\mathbf{U}_\theta, \mathbf{U}^*)] &= R_{gen}(\mathbf{U}_\theta, \mathbf{U}^*) \\ &= \int (J(\mathbf{x}, \mathbf{U}_\theta) - J(\mathbf{x}, \mathbf{U}^*)) dF(J(\mathbf{x}, \mathbf{U}_\theta)|\mathbf{x}). \end{aligned} \quad (25)$$

Where F is the probability density function of the distribution $\mathbf{x}(k)$. Then, by utilizing the inequality in (24), the probability of (21) is bounded by:

$$P\{\mathcal{L}(\mathbf{U}_\theta, \mathbf{U}^*) < \varepsilon\} \geq 1 - \frac{R_{gen}(\mathbf{U}_\theta, \mathbf{U}^*)}{\varepsilon}. \quad (26)$$

However, the generalization error $R_{gen}(\mathbf{U}_\theta, \mathbf{U}^*)$ of the learning algorithm usually cannot be determined. To deal with this issue, we derive the upper bound of $R_{gen}(\mathbf{U}_\theta, \mathbf{U}^*)$ in probability in the following.

First, we show that

$$\frac{E[\mathcal{L}^2(\mathbf{U}_\theta, \mathbf{U}^*)]}{E^2[\mathcal{L}(\mathbf{U}_\theta, \mathbf{U}^*)]} \leq c. \quad (27)$$

Because $\mathcal{L}(\mathbf{u}_\theta(\mathbf{x}), \mathbf{u}^*(\mathbf{x}))$ can be formulated as:

$$V[\mathcal{L}(\mathbf{U}_\theta, \mathbf{U}^*)] = E[\mathcal{L}^2(\mathbf{U}_\theta, \mathbf{U}^*)] - E^2[\mathcal{L}(\mathbf{U}_\theta, \mathbf{U}^*)], \quad (28)$$

it can be obtained that $c \geq 1$. Since the variance $V[\mathcal{L}(\mathbf{U}_\theta, \mathbf{U}^*)]$ is bounded and greater than zero [37], there exists a positive integer $c \geq 1$ such that the inequality in (27) holds. Since $\mathcal{L}(\mathbf{U}_\theta, \mathbf{U}^*) \geq 0$ and $\mathbf{x}(k)$ satisfy a uniform distribution, we have:

$$E[\mathcal{L}^2(\mathbf{U}_\theta, \mathbf{U}^*)] \geq \frac{4}{3} E^2[\mathcal{L}(\mathbf{U}_\theta, \mathbf{U}^*)], \quad (29)$$

c can take the value $c = 2$.

Then, substituting (27) into (29), we obtain:

$$\begin{aligned} V[\mathcal{L}(\mathbf{U}_\theta, \mathbf{U}^*)] &\leq (c-1)E^2[\mathcal{L}(\mathbf{U}_\theta, \mathbf{U}^*)] \\ &\leq (c-1)R_{gen}^2(\mathbf{U}_\theta, \mathbf{U}^*). \end{aligned} \quad (30)$$

Next, by using the inequality in (30), the upper bound of the variance of $R_{emp}(\mathbf{U}_\theta, \mathbf{U}^*)$ can be calculated as:

$$\begin{aligned} V[R_{emp}(\mathbf{U}_\theta, \mathbf{U}^*)] \\ = V\left[\frac{1}{M} \sum_{k=1}^M (J(\mathbf{x}(k), \mathbf{U}_\theta(k)) - J(\mathbf{x}(k), \mathbf{U}^*(k)))\right] \\ = \frac{1}{M^2} \sum_{k=1}^M V[(J(\mathbf{x}(k), \mathbf{U}_\theta(k)) - J(\mathbf{x}(k), \mathbf{U}^*(k)))] \\ = \frac{1}{M} V[\mathcal{L}(\mathbf{U}_\theta, \mathbf{U}^*)] \\ \leq \frac{c-1}{M} R_{gen}^2(\mathbf{U}_\theta, \mathbf{U}^*). \end{aligned} \quad (31)$$

In addition, the expectation of $R_{emp}(\mathbf{U}_\theta, \mathbf{U}^*)$ can be calculated as:

$$\begin{aligned} E[R_{emp}(\mathbf{U}_\theta, \mathbf{U}^*)] \\ = E\left[\frac{1}{M} \sum_{k=1}^M (J(\mathbf{x}(k), \mathbf{U}_\theta(k)) - J(\mathbf{x}(k), \mathbf{U}^*(k)))\right] \\ = \frac{1}{M} \sum_{k=1}^M E[(J(\mathbf{x}(k), \mathbf{U}_\theta(k)) - J(\mathbf{x}(k), \mathbf{U}^*(k)))] \\ = \frac{1}{M} \sum_{k=1}^M R_{gen}(\mathbf{U}_\theta, \mathbf{U}^*) = R_{gen}(\mathbf{U}_\theta, \mathbf{U}^*). \end{aligned} \quad (32)$$

By combining the inequality in (31) and (32), we can get:

$$\begin{aligned} P\{|R_{emp}(\mathbf{U}_\theta, \mathbf{U}^*) - R_{gen}(\mathbf{U}_\theta, \mathbf{U}^*)| < \sigma\} \\ \geq 1 - \frac{(c-1)R_{gen}^2(\mathbf{U}_\theta, \mathbf{U}^*)}{\sigma^2 M} \end{aligned} \quad (33)$$

where the Chebyshev inequality is utilized.

Setting σ as $\sigma = \sqrt{\frac{c-1}{M\delta}} R_{gen}(\mathbf{U}_\theta, \mathbf{U}^*)$ and substituting it into (33), we have:

$$\begin{aligned} P\{|R_{emp}(\mathbf{U}_\theta, \mathbf{U}^*) - R_{gen}(\mathbf{U}_\theta, \mathbf{U}^*)| \\ < \sqrt{\frac{c-1}{M\delta}} R_{gen}(\mathbf{U}_\theta, \mathbf{U}^*)\} \geq 1 - \delta. \end{aligned} \quad (34)$$

Finally, considering that the empirical error is less than the generalization error [38], the upper bound of $R_{gen}(\mathbf{U}_\theta, \mathbf{U}^*)$ satisfies the following:

$$P\{R_{gen}(\mathbf{U}_\theta, \mathbf{U}^*) \leq (1 - \sqrt{\frac{c-1}{M\delta}})^{-1} R_{emp}(\mathbf{U}_\theta, \mathbf{U}^*)\} \geq 1 - \delta. \quad (35)$$

When $\delta \rightarrow 0$ and the number of training samples M is large enough, the probability of $R_{gen}(\mathbf{U}_\theta, \mathbf{U}^*) \leq (1 - \sqrt{\frac{c-1}{M\delta}})^{-1} R_{emp}(\mathbf{U}_\theta, \mathbf{U}^*)$ approaches to 1. Applying (35) into (26), the inequality in (22) is derived, which completes the proof. \square

Remark 2: (31) and (32) require the training sampling data \mathbf{x}_k to be independently and identically distributed (i.i.d), which are widely used in machine learning algorithms [39], [40]. In this paper, we set the data buffer and uniform random sampling to ensure the uniform distribution and i.i.d. property of the training sampling data.

Next, the asymptotic stability in probability of the closed-loop system with the learned policy is presented.

Theorem 2: Suppose that Assumptions 1-3 hold, consider any state region $\mathcal{X}_0 \subseteq \mathcal{X}_f$. Then the closed-loop system (1) under the suboptimal control policy \mathbf{U}_θ obtained by Algorithm 2 and Algorithm 3 is asymptotically stable in probability.

Proof 2: Consider that the system state is $\mathbf{x}(k)$, and the feasible suboptimal solution obtained from DNN is $\mathbf{U}_\theta(k) = [\mathbf{u}_\theta(k; k), \dots, \mathbf{u}_\theta(k + N - 1; k)]$. Then we can get the state of the next moment $\mathbf{x}(k + 1) = \mathbf{f}(\mathbf{x}(k), \mathbf{u}_\theta(k; k))$. For state $\mathbf{x}(k + 1)$, there is a feasible control input sequence $\mathbf{U}_\theta(k + 1) = [\mathbf{u}_\theta(k + 1; k), \dots, \mathbf{u}_\theta(k + N - 1; k), \mathbf{v}]$ due to Assumptions 3, where $\mathbf{v} = \kappa(\tilde{\mathbf{x}}(k + N; k))$. According to [41], we can get the following inequality:

$$\begin{aligned} J(\mathbf{x}(k + 1), \mathbf{U}^*(k + 1)) &\leq J(\mathbf{x}(k + 1), \mathbf{U}_\theta(k + 1)) \\ &= J(\mathbf{x}(k), \mathbf{U}_\theta(k)) + (\|\tilde{\mathbf{x}}(k + N; k)\|_Q^2 + \|\mathbf{v}\|_R^2) \\ &\quad - (\|\mathbf{x}(k; k)\|_Q^2 + \|\mathbf{u}(k; k)\|_R^2) \\ &\quad + \|\tilde{\mathbf{x}}(k + N + 1; k)\|_P^2 - \|\tilde{\mathbf{x}}(k + N; k)\|_P^2. \end{aligned} \quad (36)$$

Here, $\mathbf{U}^*(k + 1) = [\tilde{\mathbf{u}}^*(k + 1; k), \dots, \tilde{\mathbf{u}}^*(k + N; k)]$ is the optimal solution. According to Assumption 3, it follows that:

$$J(\mathbf{x}(k + 1), \mathbf{U}^*(k + 1)) - J(\mathbf{x}(k), \mathbf{U}_\theta(k)) \leq -(\|\mathbf{x}(k)\|_Q^2 + \|\mathbf{u}(k)\|_R^2). \quad (37)$$

Using Theorem 1, when the sampling number M is large enough, then there is small enough $\varepsilon > 0$, such that $\mathcal{L}(\mathbf{U}_\theta, \mathbf{U}^*) < \varepsilon \leq \max_{\mathbf{x} \in \mathcal{X}_0} \|\mathbf{x}\|_Q^2$. Then we can get $J(\mathbf{x}, \mathbf{U}_\theta) < J(\mathbf{x}, \mathbf{U}^*) + \max_{\mathbf{x} \in \mathcal{X}_0} \|\mathbf{x}\|_Q^2$. Since $\|\mathbf{u}(k)\|_R^2 \geq 0$, the inequality (37) can be transformed into:

$$J(\mathbf{x}(k + 1), \mathbf{U}^*(k + 1)) - J(\mathbf{x}(k), \mathbf{U}^*(k)) < \max_{\mathbf{x} \in \mathcal{X}_0} \|\mathbf{x}\|_Q^2 - \|\mathbf{x}(k)\|_Q^2. \quad (38)$$

For $\mathbf{x}(k) \notin \mathcal{X}_0$, we can get [42]:

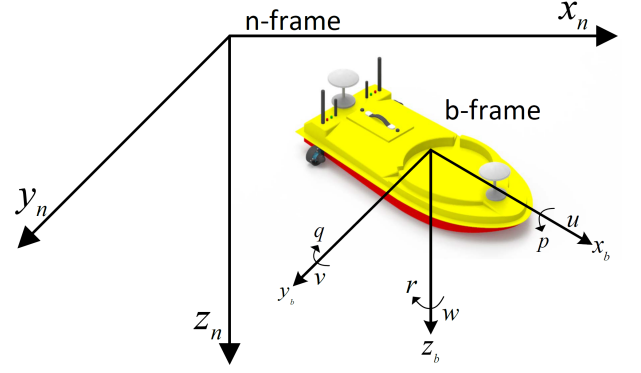


Fig. 3. State definition of unmanned surface vessel.

$$J(\mathbf{x}(k + 1), \mathbf{U}^*(k + 1)) - J(\mathbf{x}(k), \mathbf{U}^*(k)) < 0. \quad (39)$$

This indicates that the suboptimal control law is asymptotically stable with respect to a set $\mathcal{X}_0 = \{\mathbf{x} \in \mathbb{R}^n | \mathbf{x}^T \mathbf{P} \mathbf{x} \leq \gamma \alpha\} \in \mathcal{X}_f$. From this we can conclude that the closed-loop system under suboptimal control policy obtained by Algorithm 2 is asymptotically stable, because for $\mathbf{x}(k) \in \mathcal{X}_0$, $\mathbf{u}(k) = \kappa(\mathbf{x}(k))$ is a local stabilizing control policy for the closed-loop system.

Finally, from Theorem 1 it follows that, $P\{\mathcal{L}(\mathbf{U}_\theta, \mathbf{U}^*) < \max_{\mathbf{x} \in \mathcal{X}_0} \|\mathbf{x}\|_Q^2\} \rightarrow 1$. As a result, the probability that the system is asymptotically stable will also be close to 1. The proof is completed. \square

V. IMPLEMENTATION TO USVs

In this section, we implement the proposed PL-MPC algorithm for an underactuated USV.

A. USV Dynamics

To generate training data and validate performance of the proposed algorithm, we identify the model for the USV shown in Fig. 3. The USV is driven by two rear thrusters, which are T_l and T_r , respectively. The control input $F = T_l + T_r$, $M = (T_l - T_r) * d_l$, where d_l is axis distance of USV equals to 0.277m. The state space of the USV is from the north-east-down frame (n-frame) to the body frame (b-frame). It has the nonlinear discrete-time system dynamics as follows:

$$\begin{bmatrix} x_{k+1} \\ y_{k+1} \\ \psi_{k+1} \\ u_{k+1} \\ v_{k+1} \\ r_{k+1} \end{bmatrix} = \begin{bmatrix} x_k \\ y_k \\ \psi_k \\ u_k \\ v_k \\ r_k \end{bmatrix} + \Delta T \begin{bmatrix} \Delta x_k \\ \Delta y_k \\ \Delta \psi_k \\ \Delta u_k \\ \Delta v_k \\ \Delta r_k \end{bmatrix}, \quad (40)$$

where $[\Delta x_k, \Delta y_k, \Delta \psi_k, \Delta u_k, \Delta v_k, \Delta r_k]^T$ are described as:

$$\begin{bmatrix} \Delta x_k \\ \Delta y_k \\ \Delta \psi_k \end{bmatrix} = \begin{bmatrix} \cos \psi_k & -\sin \psi_k & 0 \\ \sin \psi_k & \cos \psi_k & 0 \\ 0 & 0 & 1 \end{bmatrix} \begin{bmatrix} u_k \\ v_k \\ r_k \end{bmatrix}, \quad (41)$$

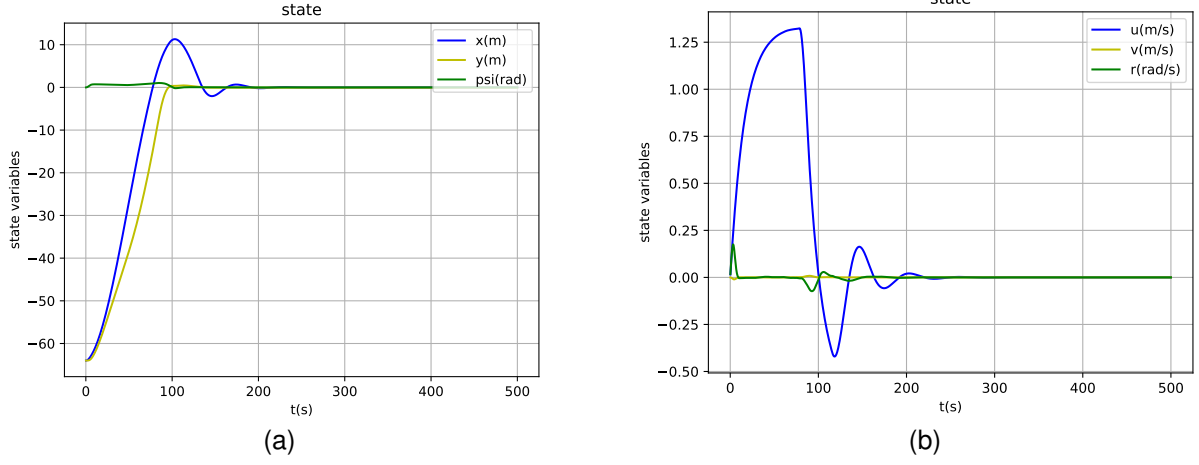


Fig. 4. State trajectory with initial system state $[-64, -64, 0, 0, 0]^T$. (a) Position trajectory. (b) Velocity trajectory.

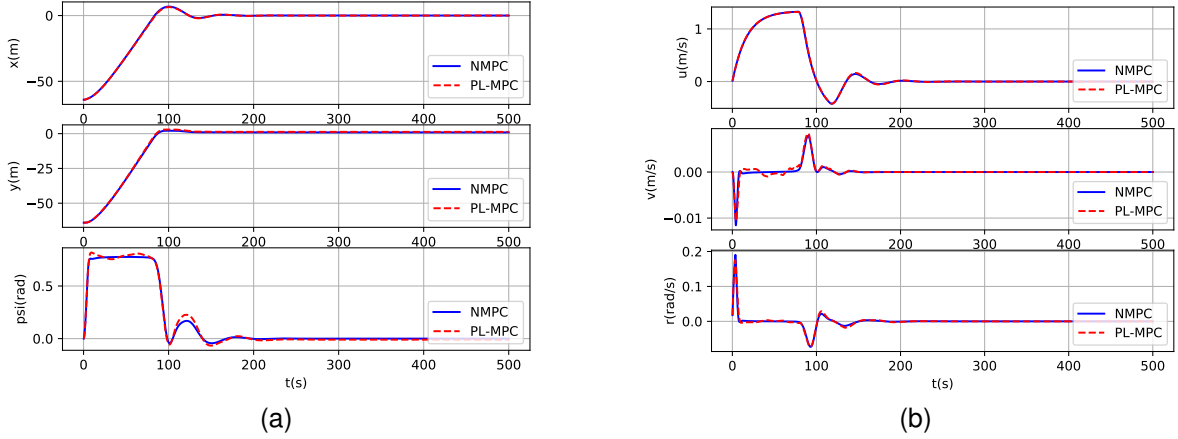


Fig. 5. Comparison of PL-MPC and NMPC algorithms. (a) Position comparison. (b) Velocity comparison.

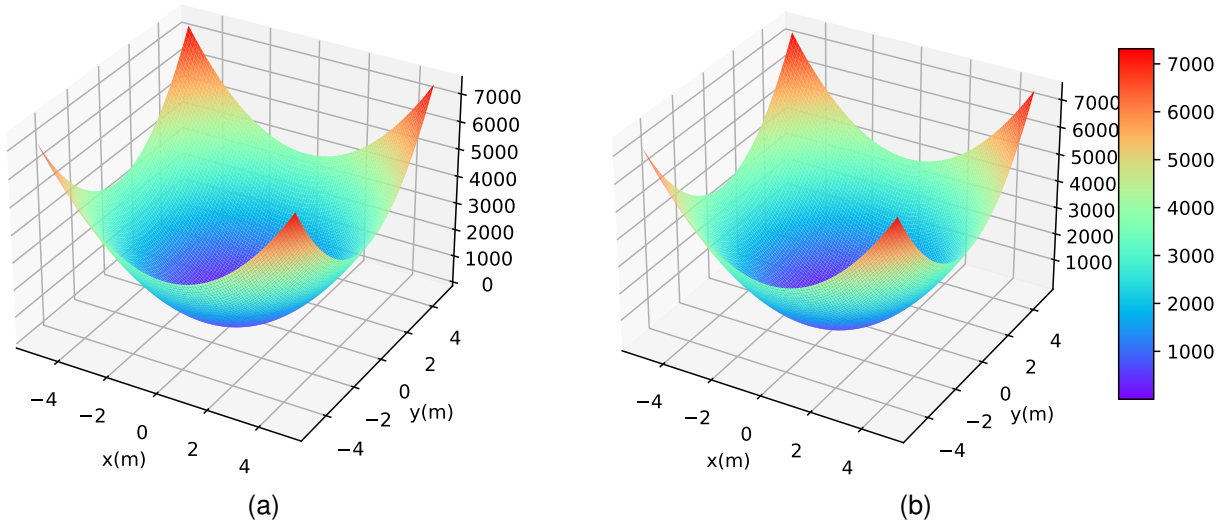


Fig. 6. Cost function with initial system state $[-5, -5, 0, 0, 0]^T$ to $[5, 5, 0, 0, 0]^T$. (a) Optimal cost function of NMPC. (b) suboptimal cost function of PL-MPC.

$$\begin{cases} \Delta u_k = (m_{22}v_k r_k - d_{11}u_k + F)/m_{11} \\ \Delta v_k = (-m_{11}u_k r_k - d_{22}v_k)/m_{22} \\ \Delta r_k = (m_{11} - m_{22})u_k v_k - d_{33}r_k + M)/m_{33} \end{cases} \quad (42)$$

Here, the state $[x_k, y_k, \psi_k]^T$ represents x-axis position, y-axis position and orientation in the n -frame, respectively. The state $[u_k, v_k, r_k]^T$ is x-axis velocity, y-axis velocity and angular velocity in the b -frame. The control input $[F, M]^T$

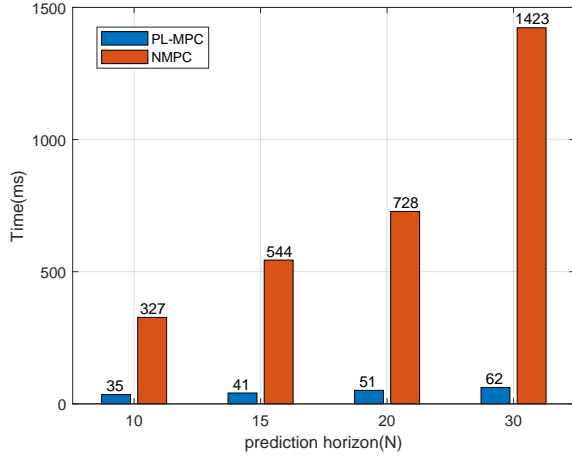


Fig. 7. Comparison computational time of PL-MPC and NMPC algorithms.

denotes the force and the torque generated by the thrusters.

By practical system identification of the USV, the system control inputs (i.e., the torque and the force limits of the two thrusters) are constrained by $-19.6N \leq F \leq 39.2N$ and $-5Nm \leq M \leq 5Nm$, respectively. The system state is constrained by $|x| \leq 70m$, $|y| \leq 70m$, $-1m/s \leq u \leq 2m/s$, $|v| \leq 1m/s$ and $|r| \leq 0.2rad/s$. $m_{11} = 493.8$, $m_{22} = 455.8$, $m_{33} = 55.8$ are the diagonal elements of the inertia matrix. $d_{11} = 29.2$, $d_{22} = 2173.7$, $d_{33} = 17.7$ are the diagonal elements of the damping matrix.

B. Learning NMPC

The training data set is generated by the traditional NMPC algorithm. The detailed parameters are: The three weighting matrices $Q = \text{diag}(10, 10, 20, 0.1, 0.1, 0.1)$, $R = \text{diag}(0.01, 0.2)$ and $P = \text{diag}(10, 10, 20, 0.1, 0.1, 0.1)$, respectively. The prediction horizon is $N = 15$. For such an underactuated USV system, the specific design of the terminal region and terminal control law $\kappa(\mathbf{x})$ can refer to [43]. The simulation nonlinear optimization problem of NMPC is solved by CasADi [44].

For DNN, the node of the input layer is set as 6, and the node of the output layer is $2N$. There are five layers in the hidden layer. Each layer has 150, 250, 250, 250 and 50 nodes, and the activation function is chosen as the ReLU function. We set $\delta = 0.01$, $\varepsilon = 0.05$ and let \mathcal{D} contain 10^6 training data, i.e., $M = 10^6$. We approximate $E[\mathcal{L}^2(\mathbf{u}_\theta(\mathbf{x}), \mathbf{u}^*(\mathbf{x}))]$ and $E[\mathcal{L}(\mathbf{u}_\theta(\mathbf{x}), \mathbf{u}^*(\mathbf{x}))]$ through the test set \mathcal{T} containing $m = 10^5$ data.

To verify the learning effect, we apply the PL-MPC algorithm to the simulation model (40) and compare it with the NMPC algorithm. Fig. 4a and Fig. 4b present the simulation trajectories with the initial system state $\mathbf{x}(0) = [-64, -64, 0, 0, 0, 0]^T$, which verifies that the closed-loop system is stable. Fig. 5a and Fig. 5b compare the system state curves of the NMPC algorithm and the proposed PL-MPC algorithm. It can be observed that the difference of the two algorithms is very small. Fig. 6a and Fig. 6b show the optimal cost function of the NMPC algorithm and the suboptimal cost

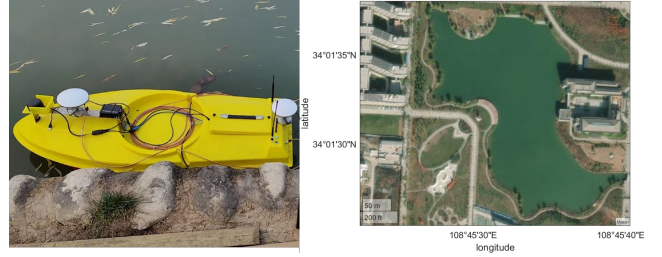


Fig. 8. USV for experimental and satellite map of experimental environment.

TABLE I
RMS VALUES OF STATE ERRORS

state error	x	y	ψ	u	v	r
RMS vlaue	0.151	0.442	0.043	0.076	0.019	0.036
unit	m	m	rad	m/s	m/s	rad/s

function of the PL-MPC algorithm, from which it can be seen that the two algorithms have almost the same cost function.

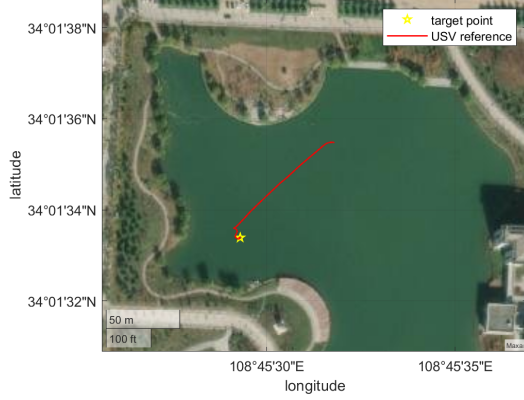
Simulations of PL-MPC and NMPC with different prediction horizons are also carried out for comparison in the same environment (CPU i7-8550U). By choosing different prediction horizons of MPC, Fig. 7 shows the detailed one-step computational time of NMPC and PL-MPC. It can be seen that, the PL-MPC algorithm greatly reduces the computation time compared with the NMPC algorithm, especially with the increase of the prediction horizon.

C. Hardware Implementation

In this section, we implement the designed PL-MPC algorithm to the USV platform and conduct the lake experiments. The experimental equipment and the environment are shown in Fig. 8. In order to verify the effectiveness of the algorithm, we have conducted two experiments corresponding to two control missions: point stabilization and trajectory tracking.

The experimental parameters of point stabilization are the same as those of simulation experiments. By training the policy using the DNN offline with data generated by simulation and deploying it for the USV, we conduct the point stabilization experiments for USV in the lake. Fig. 9a is the trajectory of USV point stabilization experiment on the map, and Fig. 9b shows the execution process of the proposed method in the experiment.

Fig. 10 shows the USV position in the experiment. Under the control algorithm, the USV can move to the equilibrium point and remain stable. Figs. 11 - 12 show the position error and velocity error, respectively. As shown in Table I, the root mean square (RMS) values of position error are $0.151m$ and $0.442m$, and the RMS value of angle error is $0.043rad$. The RMS values of velocity error are $0.076m/s$, $0.019m/s$ and $0.036rad/s$, respectively. Note that there exist unavoidably disturbances from waves and winds in the lake when the experiments were conducted. Even though the unknown disturbances, the PL-MPC controller has achieved satisfactory control performance in terms of the relatively small errors in real time experiments.



(a)



(b)

Fig. 9. USV point stabilization experiment and trajectory. (a) USV trajectory. (b) Experimental picture.

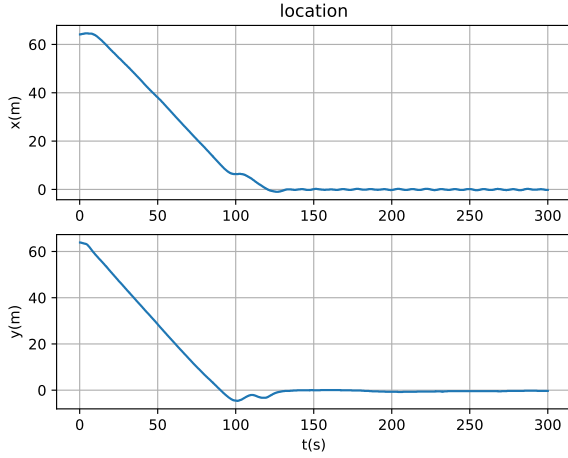
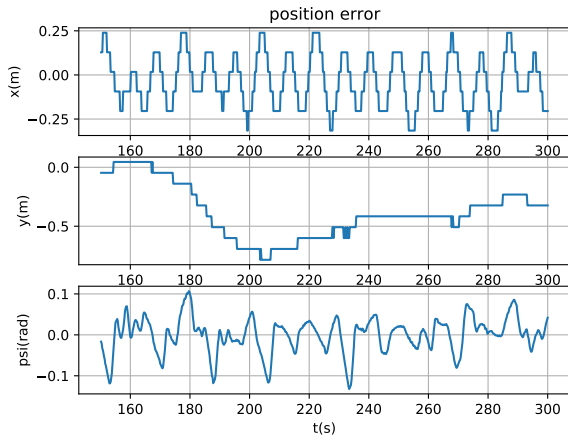
Fig. 10. Position trajectory of point stabilization experiment with initial position $[64, 64]^T$.

Fig. 11. Position error of point stabilization experiment.

For trajectory tracking experiments, we design a reference trajectory $(\mathbf{x}_d(k), \mathbf{u}_d(k))$ as a circle. The reference trajectory and USV share the same kinetic model in (40)-(42), it is denoted as $\mathbf{x}_d(k+1) = \mathbf{f}(\mathbf{x}_d(k), \mathbf{u}_d(k))$. Here, $\mathbf{x}_d(k) = [x_d(k), y_d(k), \psi(k), u_d(k), v(k), r(k)]^T$ and

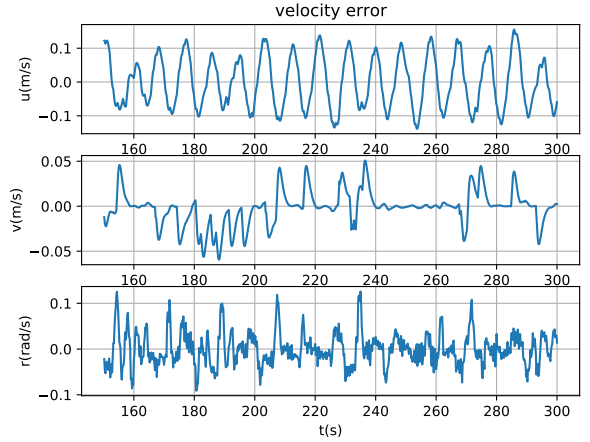


Fig. 12. Velocity error of point stabilization experiment.

$\mathbf{u}_d(k) = [F_d(k), M_d(k)]^T$. In this experiment, the reference force and moment are set as: $F_d = 17.5N$ and $M_d = 1Nm$, respectively. The reference trajectory under this control input is a circle, as shown in Fig. 14.

To track this trajectory, we define the difference between the system state and the reference trajectory state as $\mathbf{x}_e(k) = \mathbf{x}(k) - \mathbf{x}_d(k)$ and the difference between the system control input and the reference input as $\mathbf{u}_e(k) = \mathbf{u}(k) - \mathbf{u}_d(k)$.

We use \mathbf{x}_e and \mathbf{u}_e instead of \mathbf{x} and \mathbf{u} as the NMPC cost function optimization variables. Naturally, the input of the neural network changes to $\mathbf{x}_e(k)$ and the output changes to $\mathbf{U}_e(k)$, where $\mathbf{U}_e(k) = [\mathbf{u}_e(k; k), \mathbf{u}_e(k+1; k), \dots, \mathbf{u}_e(k+N-1; k)]$. The three weighting matrices $Q = \text{diag}(q_{11}, q_{22}, q_{33}, q_{44}, q_{55}, q_{66}) = \text{diag}(10, 10, 0.1, 1, 1, 1)$, $R = \text{diag}(r_{11}, r_{22}) = \text{diag}(0.01, 0.01)$ and $P = \text{diag}(10, 10, 0.1, 1, 1, 1)$, respectively. The MPC constraints and neural network parameters are the same as the simulation experiments. The terminal region and terminal control law are designed as reference [4]. We deploy the designed DNN-based policy into the trajectory control of USV, and the trajectory tracking control algorithm is executed in real time with a sampling rate at $5Hz$.

Fig. 13a is the trajectory of USV point stabilization exper-

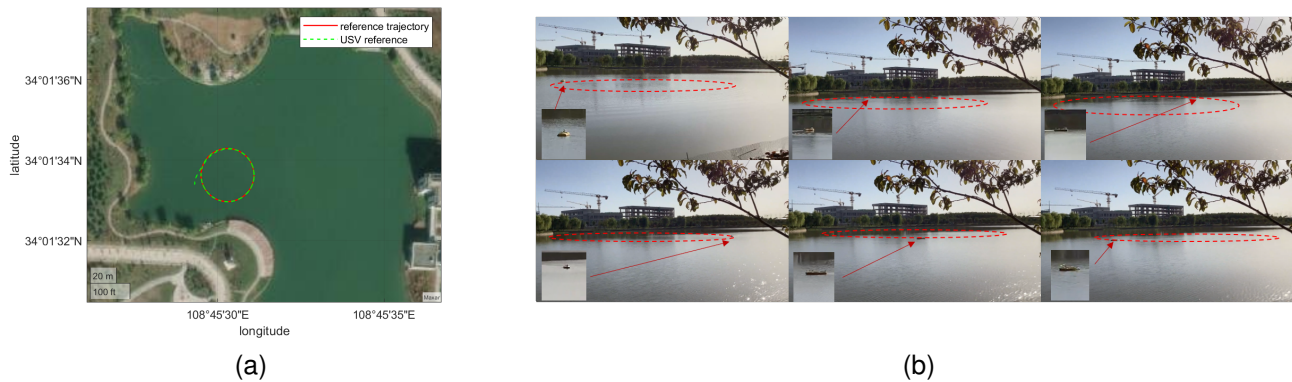


Fig. 13. USV trajectory tracking experiment and trajectory. (a) USV trajectory. (b) Experimental picture.

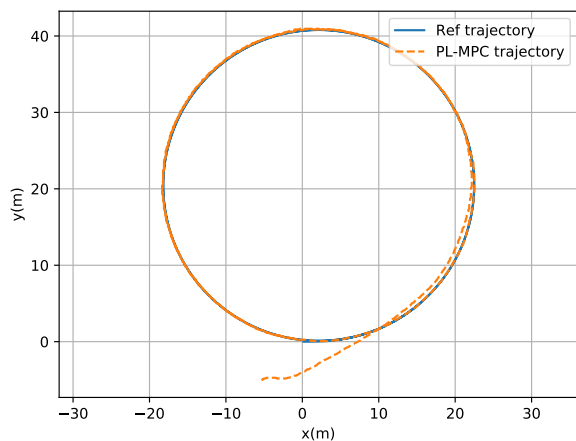


Fig. 14. Trajectory of USV with initial position $[-5, -5]^T$.

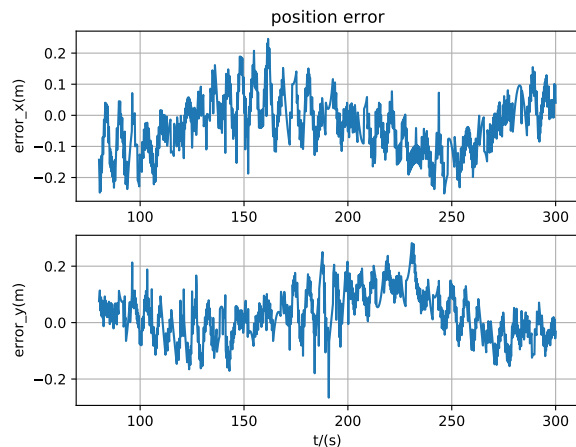


Fig. 15. Position error of trajectory tracking experiment.

iment on the map, and Fig. 13b shows the execution process of the proposed method in the experiment. Fig. 14 shows the USV position trajectory and reference trajectory, from which it can be seen that the proposed PL-MPC algorithm provides excellent tracking performance. The position errors are shown in Fig. 15 and the velocity errors are shown in Fig. 16. The RMS values of position and velocity error are $0.094m$, $0.088m$ and $0.044m/s$, $0.079m/s$ demonstrated in Table II. It can be

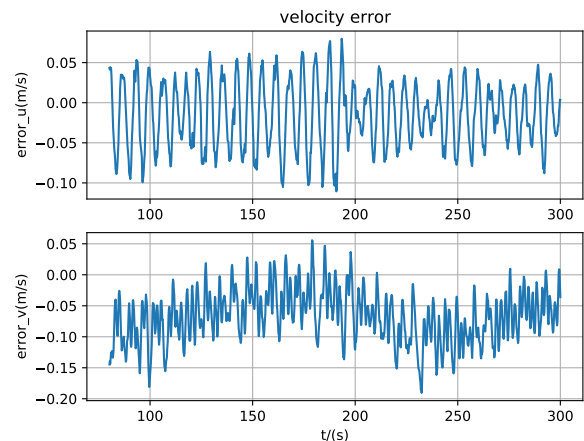


Fig. 16. Velocity error of trajectory tracking experiment.

TABLE II
RMS VALUES OF POSITION AND VELOCITY ERRORS

state error	x	y	u	v
RMS vlaue	0.094	0.088	0.044	0.079
unit	m	m	m/s	m/s

observed that the position and velocity errors under the PL-MPC algorithm are small. This verifies the effectiveness of the proposed PL-MPC algorithm in the actual environment.

VI. CONCLUSIONS

In this paper, we have developed a PL-MPC method for nonlinear discrete-time system with state and control inputs constraints, and implemented it successfully to the motion control of USVs. The DNN is trained to approximate NMPC control policy to accelerate the computational speed. By this method, we have designed the dual optimization learning algorithm, making the approximation control policies satisfy the control input and state constraints. The sufficient conditions on ensuring the closed-loop stability have also been developed. The hardware experiment for the motion control of USV have verified the feasibility and advantages of the proposed method.

REFERENCES

- [1] D. Q. Mayne, J. B. Rawlings, C. V. Rao and P. O. M. Scokaert, "Constrained model predictive control: Stability and optimality," *Control Engineering Practice*, vol. 36, no. 6, pp. 789–814, 2000.
- [2] S. Joe and T. Badgwell, "A survey of industrial model predictive control technology," *Control Engineering Practice*, vol. 11, no. 7, pp. 733–764, 2003.
- [3] A. Bemporad, D. Bernardini, R. Long, and J. Verdejo, "Model predictive control of turbocharged gasoline engines for mass production," *SAE Technical Paper*, vol. 1, no. 8, pp. 75, 2018.
- [4] H. Liang, H. Li and D. Xu, "Nonlinear model predictive trajectory tracking control of underactuated marine vehicles: theory and experiment," *IEEE Transactions on Industrial Electronics*, vol. 68, no. 5, pp. 4238–4248, 2021.
- [5] D. Wang, Q. Pan, Y. Shi, J. Hu and C. Zhao, "Efficient nonlinear model predictive control for quadrotor trajectory tracking: algorithms and experiment," *IEEE Transactions on Cybernetics*, vol. 51, no. 10, pp. 5057–5068, 2021.
- [6] M. Cannon and B. Kouvaritakis, "Continuous-time predictive control of constrained nonlinear systems," *F. Allgöwer, A. Zheng (eds) Nonlinear Model Predictive Control. Progress in Systems and Control Theory*, vol. 26, 2000.
- [7] Y. Shi, C. Shen, H. Fang, and H. Li, "Advanced control in marine mechatronic systems: A survey," *IEEE/ASME Transactions on Mechatronics*, vol. 22, no. 3, pp. 1121–1131, 2017.
- [8] C. Mark, "Efficient nonlinear model predictive control algorithms," *Annual Reviews in Control*, vol. 28, no. 2, pp. 229–237, 2004.
- [9] J. Carlo, P. Wensing, B. Katz, G. Bledt and S. Kim, "Dynamic locomotion in the MIT cheetah 3 through convex model-predictive control," in *2018 IEEE/RSJ International Conference on Intelligent Robots and Systems (IROS)*, Madrid, Spain, 2018, pp. 1–9. DOI: 10.1109/IROS.2018.8594448.
- [10] B. Katz, J. Carlo, and S. Kim, "Mini Cheetah: a platform for pushing the limits of dynamic quadruped control," in *2019 International Conference on Robotics and Automation (ICRA)*, Montreal, Canada, 2019, pp. 6295–6301. DOI: 10.1109/ICRA.2019.8793865.
- [11] P. Bemporad, *A survey on explicit model predictive control*, Berlin, Germany: Springer Berlin Heidelberg, 2007.
- [12] H. Ferreau, H. Bock and M. Diehl, "An online active set strategy to overcome the limitations of explicit MPC," *International Journal of Robust and Nonlinear Control*, vol. 18, no. 5, pp. 816–830, 2008.
- [13] P. Tondel, T. A. Johansen and A. Bemporad, "An algorithm for multiparametric quadratic programming and explicit MPC solutions," in *Proceedings of the 40th IEEE Conference on Decision and Control*, Orlando, FL, USA, 2001, pp. 1199–1204. DOI: 10.1109/CDC.2001.981048.
- [14] C. T. Wen, X. Y. Ma and B. Ydstie, "Analytical expression of explicit MPC solution via lattice piecewise-affine function," *Automatica*, vol. 39, no. 3, pp. 489–497, 2003.
- [15] E. C. Kerrigan, "Predictive control for linear and hybrid systems," *IEEE Control Systems Magazine*, vol. 38, no. 2, pp. 94–96, 2018.
- [16] L. Hewing, P. Wabersich, M. Menner and M. Zeilinger, "Learning-based model predictive control: toward safe learning in control," *Annual Review of Control, Robotics, and Autonomous Systems*, vol. 3, pp. 269–296, 2020.
- [17] A. Aswani, H. Gonzalez, S. Sastry and C. Tomlin, "Provably safe and robust learning-based model predictive control," *Automatica*, vol. 49, no. 12, pp. 16–26, 2013.
- [18] D. Limon, J. Calliess and J. Maciejowski, "Learning-based nonlinear model predictive control," *IFAC-PapersOnLine*, vol. 50, no. 1, pp. 7769–76, 2017.
- [19] P. Bouffard, A. Aswani and C. Tomlin, "Learning-based model predictive control on a quadrotor: onboard implementation and experimental results," in *2012 IEEE International Conference on Robotics and Automation*, St. Paul, MN, USA, 2012, pp. 279–284. DOI: 10.1109/ICRA.2012.6225035.
- [20] S. Bansal, R. Calandra, T. Xiao, S. Levine and C. Tomlin, "Goal-driven dynamics learning via Bayesian optimization," in *2017 IEEE 56th Annual Conference on Decision and Control (CDC)*, Melbourne, Australia, 2017, pp. 5168–5173. DOI: 10.1109/CDC.2017.8264425.
- [21] D. Piga, M. Forgiione, S. Fortentin and A. Bemporad, "Performance-oriented model learning for data-driven MPC design," *IEEE Control Syst. Lett.*, vol. 3, no. 3, pp. 577–582, 2019.
- [22] D. Gros and M. Zanon, "Data-driven economic NMPC using reinforcement learning," *IEEE Transactions on Automatic Control*, vol. 65, no. 2, pp. 636–648, 2020.
- [23] D. Rosolia and F. Borrelli, "Learning model predictive control for iterative tasks. A data-driven control framework," *IEEE Transactions on Automatic Control*, vol. 63, no. 7, pp. 1883–1896, 2018.
- [24] M. Menner, P. Worsnop and M. Zeilinger, "Constrained inverse optimal control with application to a human manipulation task," *IEEE Transactions on Control Systems*, vol. 29, no. 2, pp. 826–834, 2021.
- [25] G. Chou, D. Berenson and N. Ozay, "Learning constraints from demonstrations," *M. Morales, L. Tapia, G. Sánchez-Ante, S. Hutchinson, (eds) Algorithmic Foundations of Robotics XIII*, vol. 14, 2018.
- [26] T. Zhang, G. Kahn, S. Levine and P. Abbeel, "Learning deep control policies for autonomous aerial vehicles with MPC-guided policy search," in *2016 IEEE International Conference on Robotics and Automation (ICRA)*, Stockholm, Sweden, 2016, pp. 528–535. DOI: 10.1109/ICRA.2016.7487175.
- [27] X. Zhang, M. Bujarbaruah and F. Borrelli, "Near-optimal rapid MPC using neural networks: a primal-dual policy learning framework," *IEEE Transactions on Control Systems Technology*, vol. 29, no. 5, pp. 2102–2114, 2021.
- [28] W. Chen, T. Wang, N. Atanasov, V. Kumar and M. Morari, "Large scale model predictive control with neural networks and primal active sets," *Automatica*, vol. 135, 2022.
- [29] M. Hertneck, J. Köhler, S. Trimpe and F. Allgöwer, "Learning an approximate model predictive controller with guarantees," *IEEE Control Systems Letters*, vol. 2, no. 3, pp. 543–548, 2018.
- [30] S. Chen, K. Saulnier, N. Atanasov, D. Lee, V. Kumar, J. Pappas and M. Morari, "Approximating explicit model predictive control using constrained neural networks," in *2018 Annual American Control Conference (ACC)*, Milwaukee, WI, USA, 2018, pp. 1520–1527. DOI: 10.23919/ACC.2018.8431275.
- [31] G. Ian, B. Yoshua and H. Aaron, *Deep Learning*. Boston, MA, USA, MIT Univ. Press, 2016.
- [32] K. Hornik, M. Stinchcombe and H. White, "Multilayer feedforward networks are uni-versal approximators," *Neural Networks*, vol. 2, no. 5, pp. 359–366, 1989.
- [33] M. Leshno, V. Lin, A. Pinkus, and S. Schocken, "Multilayer feedforward networks with a nonpolynomial activation function can approximate any function," *Neural Networks*, vol. 6, no. 6, pp. 861–867, 1993.
- [34] F. Fioretto, P. Hentenryck, T. Mak, C. Tran, F. Baldo and M. Lombardi, "Lagrangian duality for constrained deep learning," *Y. Dong, G. Iffrim, D. Mladenici, C. Saunders, S. Van Hoecke, (eds) Machine Learning and Knowledge Discovery in Databases. Applied Data Science and Demo Track*, vol. 12461, 2021.
- [35] H. Chen, and F. Allgöwer, "A quasi-infinite horizon nonlinear model predictive control scheme with guaranteed stability," *Automatica*, vol. 34, no. 10, pp. 1205–1217, 1998.
- [36] D. Jakubovitz, R. Giryes, M. R. D. Rodrigues, "Generalization Error in Deep Learning," *H. Boche, G. Caire, R. Calderbank, G. Kutyniok, G. Mathar, P. Petersen, (eds) Compressed Sensing and Its Applications. Applied and Numerical Harmonic Analysis*, 2019.
- [37] Z. Yang, Y. Yu, C. You, J. Steinhardt, Y. Ma, "Rethinking bias-variance trade-off for generalization of neural networks," in *Proceedings of the 37th International Conference on Machine Learning*, Vienna, AUSTRIA, 2020, pp. 10767–10777. DOI: 10.5555/3524938.3525936.
- [38] R. Kil and K. Imhoi, "Generalization bounds for the regression of real-valued functions," in *Proceedings of the 9th International Conference on Neural Information Processing (ICONIP)*, Singapore, 2002, pp. 1766–1770. DOI: 10.1109/ICONIP.2002.1198977.
- [39] V. Mnih, K. Kavukcuoglu, D. Silver, et al, "Human-level control through deep reinforcement learning," *Nature*, vol. 518, pp. 529–533, 2015.
- [40] E. Alpaydin, *Introduction to Machine Learning*. Boston, MA, USA, MIT Univ. Press, 2004.
- [41] A. Bemporad, C. Filippi, "Suboptimal explicit MPC via approximate multiparametric quadratic programming," in *Proceedings of the 40th IEEE Conference on Decision and Control*, Orlando, FL, USA, 2001, pp. 4851–4856. DOI: 10.1109/CDC.2001.980975.
- [42] T. A. Johansen, "Approximate explicit receding horizon control of constrained nonlinear systems," *Automatica*, vol. 40, pp. 293–300, 2004.
- [43] H. P. Li, W. S. Yan, "Model Predictive Stabilization of Constrained Underactuated Autonomous Underwater Vehicles With Guaranteed Feasibility and Stability," *IEEE-ASME Transactions on Mechatronics*, vol. 22, no. 3, pp. 1185–1194, 2017.
- [44] J. Andersson, J. Gillis, G. Horn, J. Rawlings and M. Diehl, "CasADi-A software framework for nonlinear optimization and optimal control," *Mathematical Programming Computation*, vol. 11, no. 1, pp. 1–36, 2019..